Journal of Hydrology (2008) 357, 112–124

available at www.sciencedirect.com

ScienceDirect

journal homepage: www.elsevier.com/locate/jhydrol

Comparison of in-channel mobile–immobile zone exchange during instantaneous and constant rate stream tracer additions: Implications for design and interpretation of non-conservative tracer experiments

Michael N. Gooseff [a,*], Robert A. Payn [b], Jay P. Zarnetske [c], William B. Bowden [d], James P. McNamara [e], John H. Bradford [e]

[a] *Department of Civil & Environmental Engineering, Pennsylvania State University, University Park, PA 16802, United States*
[b] *Hydrologic Science & Engineering Program and Department of Geology & Geological Engineering, Colorado School of Mines, Golden, CO 80401, United States*
[c] *Department of Geosciences, Oregon State University, Corvallis, OR 97331, United States*
[d] *Rubenstein School of the Environment and Natural Resources, University of Vermont, Burlington, VT 05401, United States*
[e] *Department of Geosciences, Boise State University, Boise, ID 83725, United States*

Received 17 June 2007; received in revised form 2 May 2008; accepted 7 May 2008

KEYWORDS
Dead zone storage;
Transient storage;
Stream tracer experiment;
Arctic streams

Summary The stream tracer experiment, including field tracer application and subsequent analysis of solute transport and storage, is an important tool in stream hydrology and ecology. However, there have been few comparisons of tracer dynamics between the commonly applied methods of instantaneous (IA) and constant rate (CRA) tracer additions. To determine whether there are fundamental differences between the two addition techniques due to surface storage zone loading and flushing during experiments, we compare longitudinal distributions of tracer dynamics of stream in-channel dead zones during IA and CRA experiments. Back-to-back IA and CRA additions were carried out in two morphologically distinct tundra stream reaches in Alaska. Dead zone tracer time series are determined by an aggregate of upstream transport and individual dead zone residence time distributions (RTDs). The dead zone breakthrough curves for both tracer addition techniques were not consistent, neither were aggregate RTDs observed in each dead zone. Flushing patterns of tracer from dead zones reveal that stream flushing after IA additions was slower than after CRA additions. However, whole-stream RTDs were similar between

* Corresponding author. Tel.: +1 814 867 0044.
E-mail address: mgooseff@engr.psu.edu (M.N. Gooseff).

0022-1694/$ - see front matter
doi:10.1016/j.jhydrol.2008.05.006

IA and CRA techniques in each reach. The implications of these findings are important to design and interpretation of IA and CRA stream tracer experiments, particularly those with reactive solutes whose transformations may depend on solute concentration. Thus, IA and CRA experiments may yield differing conclusions about non-conservative transport in streams because of the inherent differences in loading of transient storage zones between these two addition techniques, and potential differences in biogeochemical processing that may occur as a consequence.

Introduction

The stream tracer experiment provides a useful characterization of stream hydraulic transport at the reach scale. Tracer experiments provide solute breakthrough curves (BTCs) from which characteristics of stream transient storage, and residence time distributions (RTDs), can be estimated. Transient storage is caused by the exchange of mobile stream water with (1) in-channel dead zones, such as side pools or eddies, and/or (2) hyporheic zones, where stream water temporarily resides in substrate pore spaces. Previous studies have focused on the influence of hyporheic exchange on transient storage (e.g., Harvey et al., 1996; Wondzell, 2006), and a few studies have focused on the influence of dead zone storage on transient storage (e.g., Hall et al., 2002). However, most studies of surface dead zone storage have been from the perspective of whole-reach response (Ensign and Doyle, 2005; Gooseff et al., 2005). Ensign and Doyle (2005), observed enhanced uptake of phosphate and ammonium due to enhanced dead zone storage in manipulation experiments, indicating that in-channel transient storage may be as important to biogeochemical cycling as hyporheic transient storage. In this paper, we characterize hydrologic storage and flushing of stream tracer from individual dead zones in two Alaskan tundra streams. Our goal is to compare dead zone BTCs and RTDs resulting from tracer additions of differing durations to determine whether there is a difference in tracer flushing behavior.

Dead zone hydrodynamics are dominated by the velocity fields created by interactions between the relatively high velocity mobile part of the channel and the slower circulation within the dead zone. Ultimately, these hydrodynamics determine the dead zone water (or tracer) residence times and exchange behavior. Thus, dead zone solute exchange (loading and flushing) depends on discharge and dead zone size. In general, these hydrodynamics are difficult to characterize because they are not consistent in space or time – dead zones do not have a consistent shape from one point to another along a channel and they experience unsteady flow regimes, altering exchange hydrodynamics through time. However, assessments of the RTDs resulting from experimental tracer flushing from dead zones may indicate the characteristics of the hydrodynamics that control tracer exchange. Before robust dead zone assessments of this kind can be made, comparisons of data acquisition technique need to be assessed. To this end, we characterize tracer RTDs observed in dead zones from different tracer addition experiment techniques. These experiments were conducted under consistent flow conditions such that the hydrodynamics are assumed consistent between experiments. We recognize that the observed RTDs in dead zones are aggregate functions of (1) upstream tracer RTDs (i.e., as a boundary condition to a dead zone of interest) and (2) the processing of tracer within the dead zone (i.e., the flushing of tracer out of the dead zone). Consequently, if differences in resulting RTD types are observed, it will be a consequence of tracer experiment type rather than specific hydrodynamic differences.

There are generally two tracer release techniques employed in field experiments. An instantaneous addition (IA), also known as a slug, gulp, or pulse, is a relatively large tracer mass instantaneously introduced to the head of an experimental reach. A constant rate addition (CRA) is a relatively small but continuous load of tracer introduced to the head of a reach over a long period of time. Intuitively, one might expect that the two tracer addition techniques differ in how they load storage zones (in-channel dead zones and hyporheic zones). However, less intuitive is how the two addition techniques relate along the studied reach. A recent analysis of whole-reach BTCs suggests that IA and CRA experiments provide similar information about whole-reach RTDs in the streams used for this study. The similarity in residence time information suggests that the bulk hydraulic retention behaved linearly with concentration and was consistent over time (Payn et al., 2008). Still unknown is how the differences between individual dead zone loading and flushing behavior of IA and CRAs influence whole-reach RTDs.

We propose that IA and CRA to differ in three ways: (1) integration of hydrologic variability, (2) longitudinal tracer loading behavior to storage zones, and (3) tracer flushing BTCs from dead zones. The IA and CRA experiments are fundamentally different because of the mass of water labeled by tracer in each. In an IA experiment, a single parcel of water in a stream reach is labeled, and the tracer data collected downstream is a legacy of where and how fast this single parcel has traveled. The CRA method requires a substantial injection duration (generally hours) to reach a steady-state downstream tracer concentration, thus in theory, labeling all parcels of water within the reach. During a CRA, it is possible that the local hydrologic conditions (such as stream discharge or near-stream groundwater levels) are not steady, especially if the addition is long (many hours to several days). Consequently, as the CRA method labels all parcels of water entering the experimental reach, each parcel may actually be responding to dynamic hydrology in or around the stream during the duration of the CRA experiment. Thus, CRA results are more likely to be a function of a more variable set of conditions than in IA experiments,

which have the advantage of labeling only a single parcel of water in the channel.

The IA and CRA experiments also differ in longitudinal tracer loading behavior to storage zones (both dead zones and the hyporheic zone). In the IA approach, loading of storage zones or the mass transfer of tracer into storage zones during the passage of a tracer plume in the thalweg, occurs with decreasing concentrations downstream due to dispersion of the tracer plume as it travels the length of the experimental reach. Due to the highly variable tracer concentrations over the duration of the IA tracer experiment, dynamic and inconsistent spatial and temporal gradients exist in tracer concentrations. When executing a CRA, unchanging concentration along the reach implies that stream-storage zone tracer gradients are also at steady-state, given relatively consistent hydrologic conditions (i.e., no change in discharge). Despite consistent tracer concentration at a given point through time (e.g., thalweg at the end of a reach), spatial variability in concentration may still exist in reach, particularly in the case of dilution from lateral inflow. If longitudinal spatial variability in concentration is substantial during a CRA, the concentrations or amounts of tracer loading of storage zones will also vary with distance downstream, but this variability is relatively small compared to the range of concentrations generated during an IA tracer experiment. Furthermore, peak thalweg and storage zone tracer concentrations along the reach should be more similar in CRA experiments than in IA experiments due to the relatively consistent gradients between the thalweg and storage zones achieved during a CRA experiment.

As soon as the IA tracer plume passes, or the CRA ends, the tracer concentration gradients between the stream and storage zones are reversed, yielding flushing of tracer from storage zones. Storage zones are subject to downstream loading of tracer originating from both the initial pulse of tracer reaching that point along the stream and from the flushing of upstream storage zones. In an IA experiment, loading in downstream storage zones is expected to be subject to high concentrations of tracer flushing from upstream storage zones. For contrast, in a CRA experiment, upstream and downstream storage zones are loaded to similar but lower peak concentrations relative to IA experiments, such that downstream loading is likely to be less substantial than upstream loading. Tracer BTCs observed in an individual storage zone is a function of the input time series (loading characteristics) and the residence time of water before returning to the mobile stream. Thus, we expect that for a single dead zone, tracer BTCs will be different during CRA and IA experiments, but that the RTDs of these two BTCs will be fundamentally similar.

In this study, we investigate stream responses to IAs and CRAs by analyzing (1) overall stream tracer flushing, and (2) longitudinal distribution of aggregate RTDs measured in dead zones. We focus on the dead zone portions of transient storage because (1) we expect them to function more comparably along the stream than any similar number of locations in the hyporheic zone, which is composed of heterogeneous flowpaths that operate on timescales that may be undetectable in CRA or IA experiments, and (2) their role in generating relatively long in-channel residence time may be critical to understanding the potential for reactive solute kinetics (e.g., biogeochemical cycling). Additionally, dead zones are easy to identify and sample non-invasively, and typically have some internal circulation to them promoting internal mixing. We test the null hypothesis that, within a given reach, there is no effective difference in aggregate RTDs of the tracer in individual dead zones between the two types of stream tracer experiments, given that all other factors (e.g. channel condition and discharge) are similar. These experiments were performed in two arctic Alaskan tundra streams of contrasting channel structure: a sinuous peat-bed stream and an alluvial gravel/cobble-bed stream.

Study site

We studied two tundra streams on the north slope of the Brooks Range in Alaska, near the Toolik Field Station (68 38′N, 149 36′W). Stream substrate in this region consists of permeable active layers that thaw through the summer, underlain by relatively impermeable permafrost. The active layer thaws to depths of 2.0+ m beneath tundra streams (Bradford et al., 2005), and tend to thaw quickly in a typical summer (Brosten et al., 2006). These thaw depths do not limit hyporheic exchange beneath these streams, except during portions of streambed thaw and freeze-up at the beginning and end of the thaw season (Zarnetske et al., 2008). The alluvial study reach length was 400 m with a slope of 0.97% and has a pool-riffle channel structure (Fig. 1). The second experimental reach was in a nearby peat-bedded stream. This reach was 250 m long with a slope of 0.90% and consisted of a beaded channel structure with wide and deep pools connected by short, deep narrow runs (Fig. 1).

Methods

Field experiments

Prior to experiments on both reaches, we selected dead zone sampling locations that would be likely to temporarily store tracer-labeled stream water. In the alluvial reach we identified the following in-channel dead zones to be sampled for RWT concentrations (all distances are downstream of injection point): (A1) eddy behind a rock at 34 m, (A2) eddy behind a boulder at 44 m, (A3) pool margin at 88 m, (A4) pool margin at 173 m, (A5) pool margin at 195 m, and (A6) pool margin at 205 m. Similarly in the peat-bedded reach, we identified the following dead zones to be sampled: (P1) eddy behind a boulder at 6 m, (P2) small side channel at 14.5 m, (P3) pool margin at 35.5 m, (P4) pool margin at 148.5 m, (P5) pool margin at 167.5 m, and (P6) pool margin at 189.5 m. At the end of each reach and for all experiments, stream RWT concentrations were measured with a Turner Designs 10-AU fluorometer (Turner Designs, Inc., Sunnyvale, CA), fitted with a flow-through cell, in-line thermometer (for temperature compensation), and data logger. Dead zones were sampled with 60-mL syringes connected to 1 m of small diameter tubing affixed to a rigid rod. This sampler design allowed us to unobtrusively sample each dead zone from the bank, with minimal perturbation of stream structure and hydraulics. Dead zone samples were

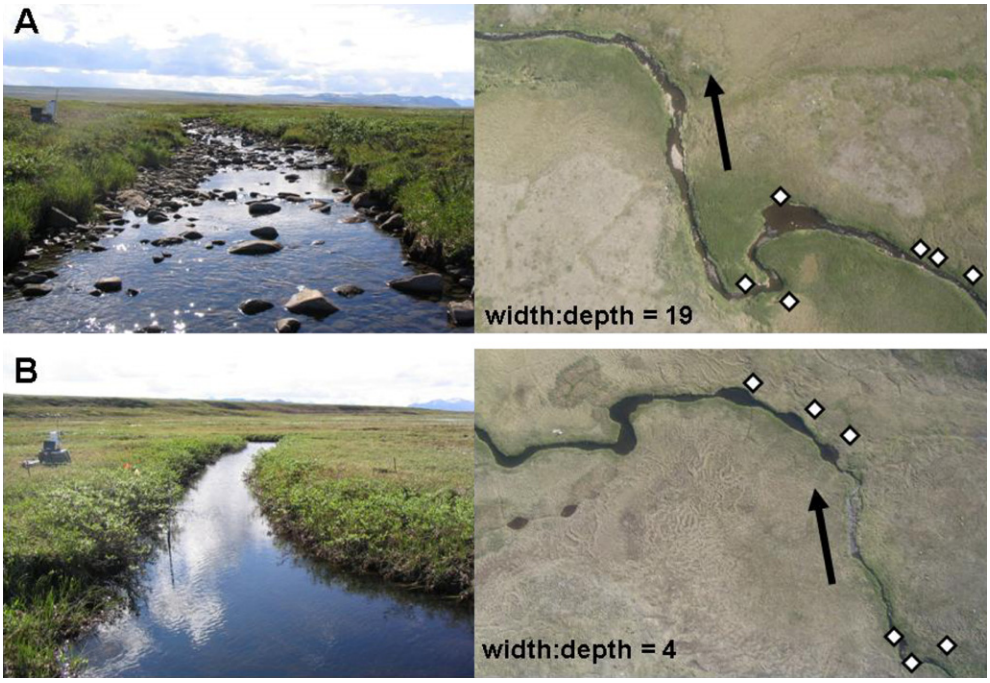

Figure 1 Field site pictures and aerial photos of (A) the alluvial reach, and (B) the peat-bedded reach. Diamonds represent dead zone sampling sites on both reaches; locations are approximate.

analyzed in a relatively constant-temperature laboratory, on the same model of fluorometer, fitted with a 13 mm diameter cuvette receptacle.

In both reaches, the experiments were run consecutively, IA then CRA, in expectation of similar hydrologic conditions for both methods. The IA experiments were started in the morning and considered complete when the downstream water returned to background fluorescence. Upon completion of the IA experiment, CRA experiments were run through the afternoon and early evening. Tracer mass for IA experiments was determined by standard mixing calculations, as presented by Fisher et al. (1979), with a target downstream concentration of 100 $\mu g\,L^{-1}$. The IA (20 g RWT powder, Bright Dyes, Inc., Miamisburg, OH dissolved in ~1 L of stream water) on the alluvial stream began at 1145 on 18 August 2004 and sampling ended around 1300; the CRA began at 1333 at a rate of 22.90 mg RWT s^{-1}, and ended at 1632. The IA on the peat-bed stream (40 g dry RWT powder dissolved in ~1 L of stream water) was released at 1131 on 16 August 2004, and sampling occurred until 1430; the CRA began at 1506 at 31.35 mg RWT s^{-1}, and ended at 1845. After the field campaign, it was discovered that the RWT powder consisted of only about 20% active ingredient. This does not affect our calculations, because the RWT product used to make calibration standards was the same as that used to make release solutions. Therefore, all RWT masses and concentrations reported are relative to the total mass of product rather than mass of the fluorescent active ingredient. Throughout each experiment, stream discharge was measured immediately downstream from the fluorometer by standard method of measuring cross-sectional velocity distributions using a Marsh-McBirney Flo-Mate 2000 current meter (Marsh-McBirney, Inc., Frederick, MD).

Tracer flushing analysis

The tracer peak passed too quickly during IAs to allow for sampling of peak dead zone or thalweg tracer concentrations. Therefore, to compare peak thalweg solute concentrations during IAs, an advection–dispersion-transient storage transport model was parameterized to the observed BTC and run at various stream lengths to estimate peak concentrations along the reach. To determine the longitudinal trend in IA peak stream tracer concentrations, we used the STAMMT-L solute transport model (Haggerty and Reeves, 2002) to simulate the whole-stream tracer BTC, and then re-ran the model at varying distances downstream with the same parameter values. During CRAs, peak concentrations were measured directly from samples collected in the thalweg and dead zones along the reach, just prior to termination of the tracer addition.

To compare stream flushing dynamics between dead zones and the whole reach, we computed regression fits for tracer concentration decrease during flushing. For the thalweg tracer data collected at the downstream outlet of the reach, we begin regressions at the peak concentrations for IA BTCs and the end of the concentration plateau for the CRA BTCs. For the dead zone BTCs, we fit equations over time since the end of the injection common to both IA and CRA experiments in each stream. The linear and nonlinear regression fits were computed using spreadsheet software. We chose to regress only over timescales that did not include initial high concentrations because there were very different peak concentrations during each experiment. Thus, for BTCs observed in dead zones, single outlier values may unduly bias the regressions even within the same individual dead zone between CRA and IA responses. Furthermore, we report only the best-fit regression equations (as

determined by the highest coefficient of determination, R^2, values), chosen from three types: linear, exponential, and power-law functions. In all cases, regressions were developed for a minimum of six data points.

The observed time series of tracer concentrations in each dead zone represents an aggregate of two RTDs. First, the upstream RTD characterizes stream transport from the injection point to the loading point of a given dead zone. Second the dead zone RTD characterizes the function of the individual dead zone that convolves with its loading behavior to generate the observed flushing response. To compare the IA and CRA responses, we compared the equation of the best-fit regression of the IA concentration time series in each dead zone with the derivative of the best-fit regression of the CRA time series data in each dead zone. Using the derivative of the CRA data assumes a step function (''step-down'' or inverted Heaviside function) at the head of the reach, which is subsequently processed by the RTD of stream transport and the RTD of the individually sampled dead zone. The derivative of a step-response is equivalent to the RTD if the hydraulic retention behavior can be characterized with linear models. Because a normalized BTC of an IA is inherently equivalent to an RTD, comparing the IA response with the derivative of the CRA response allows direct comparison of stream behavior. We denote these aggregated residence time functions as Θ_{IA} and Θ_{CRA}, respectively. Though it would be desirable, it is not possible to meaningfully disaggregate upstream and dead zone behavior without thalweg tracer concentration data just outside of each dead zone, which could have been used to characterize the upstream RTD. Because RTDs from downstream thalweg tracer concentrations are equivalent between IA and CRA experiments (Payn et al., 2008), we expect that differences in Θ_{IA} and Θ_{CRA} will be indicative of differences in the operation of each dead zone. However, without the thalweg BTCs collected at each dead zone, this approach is not definitive.

Results

The average stream discharges, measured by velocity cross-sections during IA and CRA experiments, were similar for both experiments in each reach. Average discharges during the alluvial stream IA and CRA experiments were 351 L s^{-1} and 363 L s^{-1}, respectively. Average discharge during the IA experiment in the peat-bed stream was 254 L s^{-1}, whereas during the CRA experiment the discharge was 280 L s^{-1}.

Differences between the IA and CRA experimental techniques were evident in two patterns of peak tracer concentrations: (1) the peak tracer concentrations at the end of the reach and (2) the longitudinal profiles of peak tracer concentrations along the thalweg of the stream. The peak RWT concentration at the end of the alluvial reach was higher for the IA than for the CRA experiment (Fig. 2A). At the end of the peat-bedded reach, the peak CRA tracer concentration was slightly greater than that of the IA experiment (Fig. 2B). In both the alluvial and peat-bed stream reaches, the estimated longitudinal distribution of peak stream tracer concentrations were generally much higher during the IA experiments than those sampled during the observed plateau conditions of CRA experiments (Fig. 3). During CRA tracer concentration plateau conditions in both reaches, the longitudinal stream tracer concentrations were fairly consistent except for minor apparent dilution toward the end of the alluvial reach (Fig. 3A) and near the head of the peat-bed reach (Fig. 3B). These dilutions of mobile stream water indicate a variable distribution of lateral inflow in each reach.

Tracer breakthrough curve regression analysis

Regressions of tracer concentrations at the end of the alluvial reach were best-fit by power-law functions with exponents of −5.2 and −18.7 for the IA and CRA experiments, respectively (Fig. 4A and B), whereas in the peat-bedded reach, best-fit regressions were found to be exponential functions with similar exponents, $-0.06t$ for IA, $-0.07t$ for CRA (Fig. 4C and D). These results are consistent with those of Payn et al. (2008) who found that the RTDs from IA and CRA experiments were equivalent in both reaches, however, our gross regressions from peak tracer concentrations probably account for the differences in power-law exponents for the alluvial reach. These results are also consistent with those of Zarnetske et al. (2007), who note that in repeated IA stream tracer experiments in several arctic

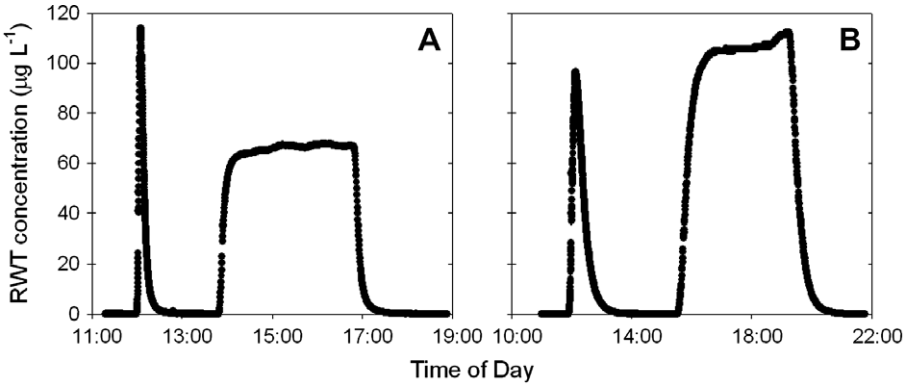

Figure 2 Rhodamine WT breakthrough curves, as collected at the end of each reach, for (A) alluvial reach, on 18 August 2004, and (B) peat-bedded reach, on 16 August 2004. Gaps in the breakthrough curves are due to changes in sensitivity ranges of the field fluorometer.

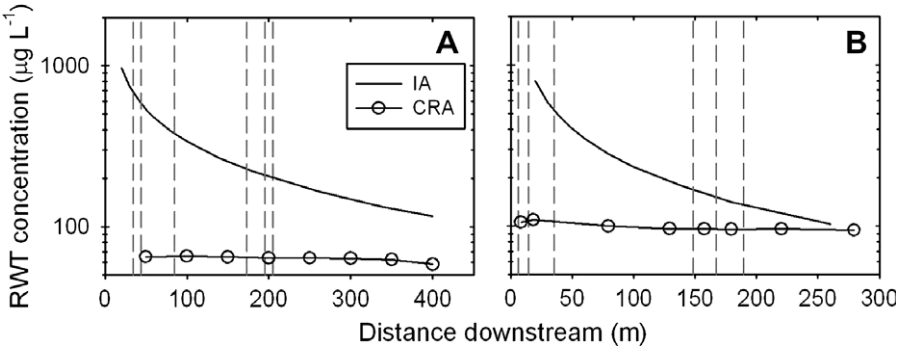

Figure 3 Longitudinal peak Rhodamine WT concentrations in the mobile stream water for (A) alluvial and (B) peat-bedded experimental reaches. Peak instantaneous addition (IA) concentrations are estimated using solute transport simulations, and constant rate addition (CRA) maximum concentrations were sampled during the experiment (symbols on plot). Vertical dashed lines indicate dead-zone sampling locations.

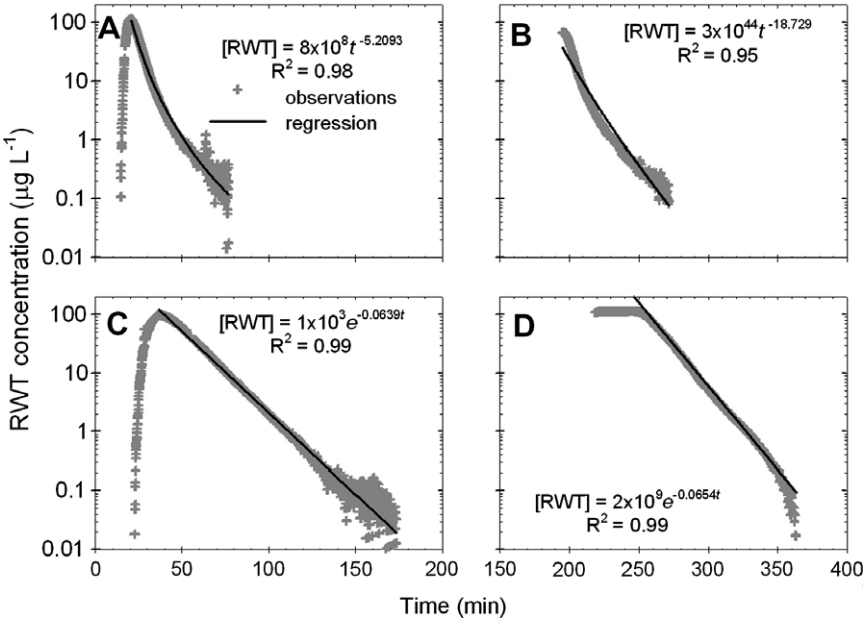

Figure 4 Regression fits to late-time BTC data from the downstream thalweg in the alluvial reach: (A) IA experiment, (B) CRA experiment, and in the peat-lined reach: (C) IA experiment, and (D) CRA experiment. Best-fit regression type equation (as determined by maximum R^2) and resulting R^2 value are provided.

tundra streams (including these two), alluvial reaches generally demonstrate power-law flushing behavior, and peat-bedded reaches generally demonstrate exponential flushing behavior. Our comparisons of the regression functions of tracer data collected at the end of the reach focus on the exponents of the functions, because, for both power-law and exponential regressions, the negative exponent of the function influences of the shape of decay in the function. As intercepts in various log-transformed spaces, the coefficients in these functions generally offset the magnitude of the function. Thus we compare only the exponents of these functions to seek similarity in the aggregate flushing dynamics measured in each dead zone (i.e., we expect the function coefficients to more likely to be different between IA and CRA experiments for the same dead zone).

In both study streams, dead zones were subject to different peak concentrations (higher in upstream dead zones than downstream dead zones), and yet similar dead zone flushing dynamics resulted from IA and CRA experiments (Figs. 5 and 6). The dead zones in the alluvial reach flushed tracer similarly over the 50–140 min period of sampling after the passing of the peak tracer concentrations in each experiment (Fig. 5). In general, the alluvial dead zones had higher concentrations that were sustained for longer in the IA tracer experiment relative to the CRA experiment, particularly in the upstream dead zones. The flushing characteristics in alluvial dead zones were best represented by power-law regressions in all but A4, which was best-fit with an exponential regression (Table 1, Fig. 5). In all 5 of the power-law cases, the exponent of the best-fit function in IA flushing response was greater in magnitude (more negative) than that of the CRA flushing regression, suggesting a more rapid aggregate flushing effect in dead zones. The flushing slopes of the exponential regressions (exponent coefficient) at A4 were similar for both experiments.

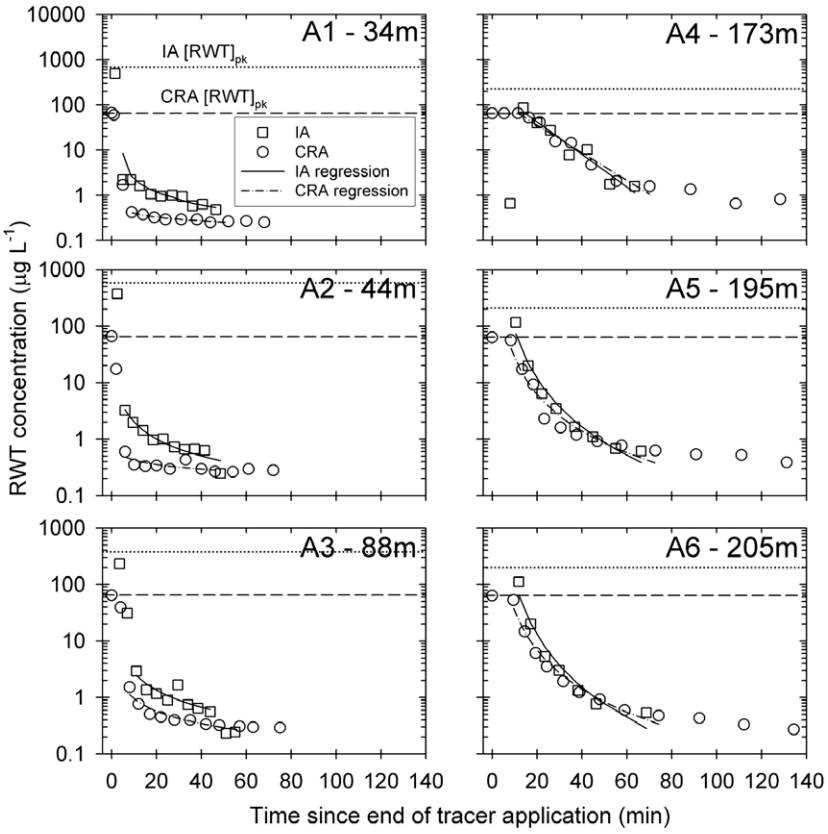

Figure 5 Rhodamine WT concentrations sampled from alluvial reach dead zones on 18 August 2004: (A1) eddy behind a boulder at 34 m, (A2) eddy behind a boulder at 44 m, (A3) pool margin at 88 m, (A4) pool margin at 173 m, (A5) pool margin at 195 m, and (A6) pool margin at 205 m downstream of the injection location. Trend lines for each storage zone are best-fit lines determined using spreadsheet software, only where IA (open squares) and CRA (open circles) data overlap in time since the end of the injection. Trend line equations and coefficients of determination (R^2) are documented in Table 1.

Analogous dead zone dynamics were observed in the peat-bedded reach, except that all BTCs in peat-bedded reach dead zones were best regressed with power-law functions (Table 1). Upstream dead zones tend to have initially higher RWT concentrations during the IA experiments than during the CRA experiments (Fig. 6). In the downstream dead zones, flushing responses following both IA and CRA injections are visually comparable, nearly plotting on top of each other (Fig. 6, P4—P6). For the peat-bedded stream IA experiment, a downstream increase of power-law exponent magnitudes exists from P2 to P6, increasing from −0.720 to −3.29. However, in the peat-bedded reach CRA experiment this pattern is inconsistent with an increasing trend from side channel P2 to pool margin P4, but a drop in the regression at dead zone P5. Similar to the alluvial reach, the magnitude power-law exponents is generally greater for the IA experiment than for the CRA experiment, except in the case of P4, a pool margin.

Dead zone residence time analyses

As with the flushing BTC fits, the aggregate RTDs (Θ) in each dead zone are characterized by differences within each dead zone and systematic downstream trends. A comparison of Θ within each dead zone is facilitated by comparing the exponents of Θ_{IA} and Θ_{CRA} in Table 1. For all alluvial dead zones except A4, the Θ_{CRA} exponents are similar, but slightly greater than the corresponding Θ_{IA}. The mean and standard deviation of the Θ_{IA} exponents for the alluvial reach (except A4) are -1.75 ± 1.12, and for Θ_{CRA}, -2.15 ± 1.01. In A4, the power of the exponential function of Θ_{IA} is slightly greater than the power in the corresponding Θ_{CRA} function. In the peat-bed reach experiments, the exponents of Θ_{CRA} for all dead zones are greater than for corresponding Θ_{IA} (except in P4), though these differences are greater than observed in the alluvial reach. The mean and standard deviation of the Θ_{IA} exponents for the peat-bed reach are -1.92 ± 1.18, and for Θ_{CRA}, -2.44 ± 0.95. The normalized Θ plots also reflect this standard deviation interpretation because the alluvial Θ_{IA} and Θ_{CRA} plots are much more similar (Fig. 7) than those in the peat-bed reach, except for P4 and P5, in which Θ_{IA} and Θ_{CRA} plot very close to each other (Fig. 8). In both reaches, both Θ_{IA} and Θ_{CRA} along the reach reflect increasing exponent magnitudes downstream.

Discussion

Dead zone and whole-stream flushing behavior

Our expectation that IA and CRA experiments would yield similar whole-stream flushing is supported by the reach scale transport of tracer in the peat-bedded reach, as both

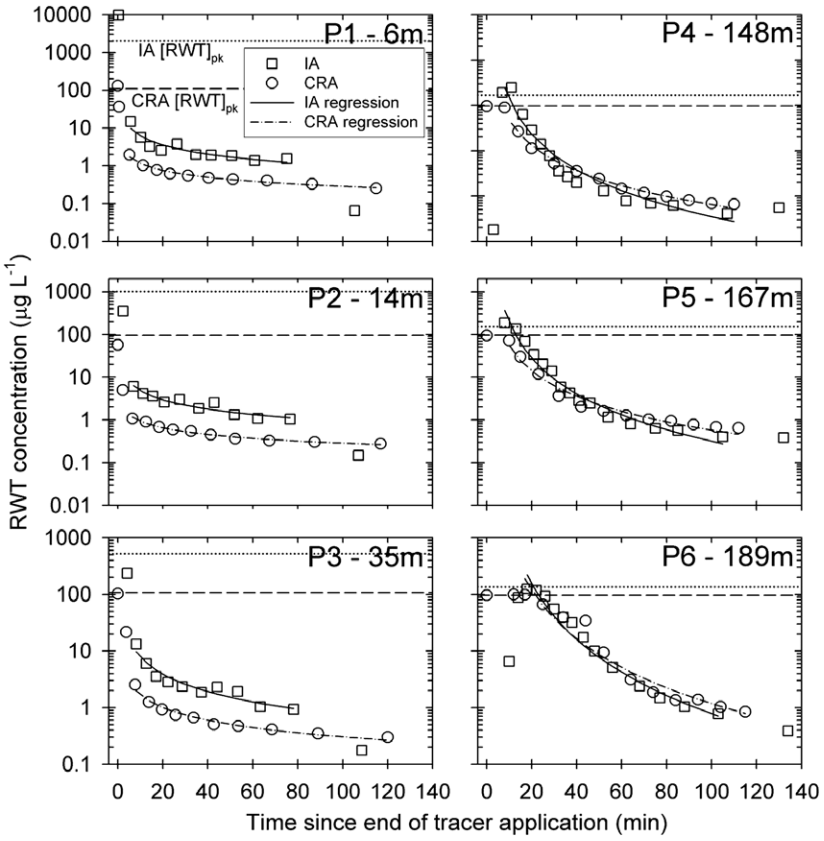

Figure 6 Rhodamine WT concentrations sampled from peat-bedded reach dead zones on 16 August 2004: (P1) eddy behind a boulder at 6 m, (P2) small side channel at 14 m, (P3) pool margin at 35 m, (P4) pool margin at 148 m, (P5) pool margin at 167 m, and (P6) pool margin at 189 m downstream of the injection location. Trend lines for each storage zone are best-fit lines determined using spreadsheet software, only where IA (open squares) and CRA (open circles) data overlap in time since the end of the injection. Trend line equations and coefficients of determination (R^2) are documented in Table 1.

the IA and CRA whole-stream regressions at the end of the reach are similar (Fig. 4). The power-law regression exponents of the flushing patterns for the IA and CRA experiments in the alluvial reach are quite different though (Fig. 4), indicating somewhat similar flushing behavior, but at different rates. We are confident that the effects of

Table 1 Flushing regressions of stream-storage zone concentrations sampled during IA and CRA experiments

Storage site	Distance downstream (m)	Storage zone type	IA experiment flushing equation, Γ_{IA} (R^2)	CRA experiment flushing equation (R^2)	Θ_{CRA}
Alluvial reach					
A1	34	Eddy	$C = 12.9t^{-0.825}$ (0.93)	$C = 0.76t^{-0.279}$ (0.92)	$-0.212t^{-1.28}$
A2	44	Eddy	$C = 19.6t^{-0.993}$ (0.96)	$C = 0.78t^{-0.261}$ (0.51)	$-0.202t^{-1.26}$
A3	88	Pool margin	$C = 27.3t^{-1.00}$ (0.75)	$C = 5.14t^{-0.734}$ (0.89)	$-3.77t^{-1.73}$
A4	173	Pool margin	$C = 220e^{-0.083t}$ (0.94)	$C = 145e^{-0.070t}$ (0.96)	$-10.2e^{-0.070t}$
A5	195	Pool margin	$C = 5.86 \times 10^4 t^{-2.84}$ (0.97)	$C = 3.94 \times 10^3 t^{-2.16}$ (0.94)	$-8.51 \times 10^3 t^{-3.16}$
A6	205	Pool margin	$C = 1.39 \times 10^5 t^{-3.10}$ (0.95)	$C = 4.35 \times 10^4 t^{-2.98}$ (0.98)	$-1.53 \times 10^4 t^{-3.30}$
Peat-bedded reach					
P1	6	Eddy	$C = 39.6t^{-0.805}$ (0.87)	$C = 4.66\ t^{-0.609}$ (0.98)	$-2.83t^{-1.61}$
P2	14	Side channel	$C = 25.7t^{-0.720}$ (0.91)	$C = 3.06t^{-0.520}$(0.98)	$-1.58t^{-1.52}$
P3	35	Pool margin	$C = 84.4t^{-1.03}$ (0.92)	$C = 197t^{-0.745}$(0.97)	$-147t^{-1.75}$
P4	148	Pool margin	$C = 1.28 \times 10^5\ t^{-2.86}$ (0.99)	$C = 3.66 \times 10^3 t^{-1.88}$ (0.92)	$-6.87 \times 10^3 t^{-2.88}$
P5	167	Pool margin	$C = 1.21 \times 10^5 t^{-2.79}$ (0.97)	$C = 5.29 \times 10^3 t^{-1.98}$ (0.97)	$-1.05 \times 10^4 t^{-2.98}$
P6	189	Pool margin	$C = 3.00 \times 10^6 t^{-3.29}$ (0.98)	$C = 6.40 \times 10^5 t^{-2.87}$ (0.94)	$-1.84 \times 10^6 t^{-3.87}$

Flushing equations apply to trend lines plotted in Figs. 5 and 6, where time is measured in minutes, and Θ (normalized to an initial value of 1.0) equations are plotted in Figs. 7 and 8.

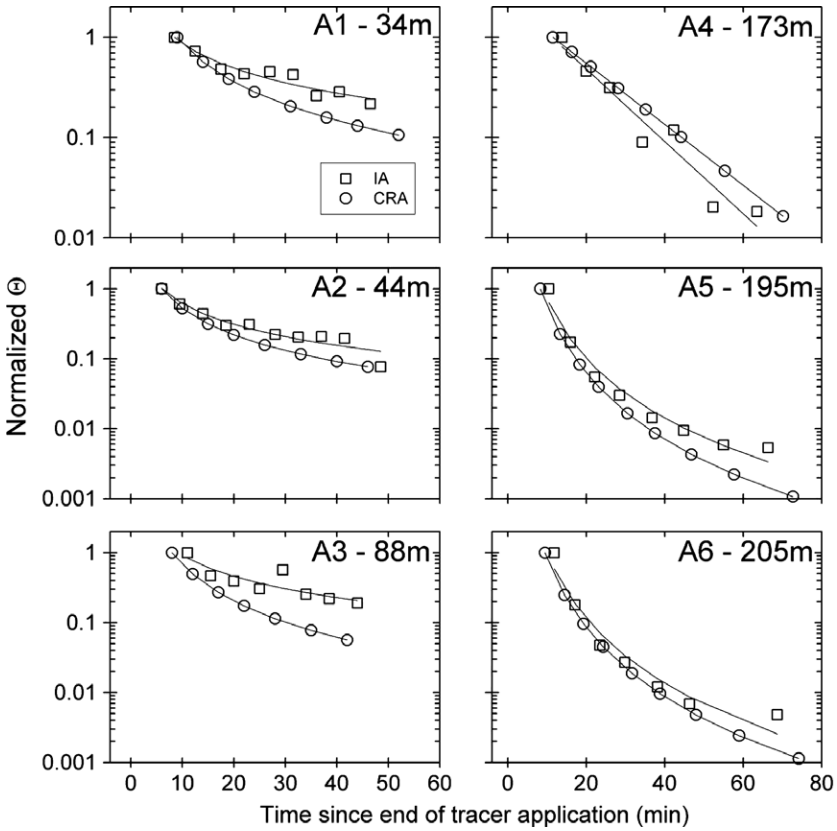

Figure 7 Normalized residence time functions Θ_{IA} and Θ_{CRA} from alluvial reach dead zones (A1) eddy behind a boulder at 34 m, (A2) eddy behind a boulder at 44 m, (A3) pool margin at 88 m, (A4) pool margin at 173 m, (A5) pool margin at 195 m, and (A6) pool margin at 205 m downstream of the injection location. Symbols represent discrete times of sampling, and lines are the functions identified in Table 1. All data are normalized to the first value being a Θ value of 1.0 for each time series.

RWT sorption to streambed material did not differentially influence the RTDs (i.e., IA vs. CRA) we observed because previous studies have shown that the sorption isotherm is linear (e.g., Gooseff et al., 2005), and because the results of Payn et al. (2008) reported that a non-parametric analysis of the RTDs for the same set of stream tracer experiments indicated that IA and CRA RTDs are comparable within each reach. Had there been a significant non-linear RWT sorption/desorption influence on the whole-stream BTCs, the corresponding RTDs in each reach would not have been so similar. Furthermore, the comparisons of IA and CRA in the same reach facilitate comparisons between the techniques because the CRA was performed immediately after the IA, in an effort to replicate consistent flow and channel conditions. It is surprising how consistent the peat-bedded reach demonstrated exponential slopes in the tails of both whole-stream BTCs, which agree well with the analysis of deconvolved RTDs from Payn et al. (2008).

Despite similarities in whole-reach responses, the flushing dynamics of individual dead zones in both reaches indicate that there is dissimilar localized storage behavior in response to IA and CRA experiments. Firstly, the difference in dead zone flushing BTC trends between IA and CRA experiments in both reaches (Figs. 5 and 6) suggests that aggregate responses are different for each experiment type. Secondly, the Θ_{CRA} power function exponents are consistently larger in magnitude than Θ_{IA} exponents for the aggregate RTDs in both reaches (Table 1). While this is a consistent trend, a comparison of the average and standard deviations of exponent values of the Θ functions indicates that the exponent groups are significantly different (two-tailed paired t-tests, $\alpha = 0.05$, for comparisons of exponents: $p = 0.014$ in alluvial reach, $p = 0.013$ in peat-bed reach). One possible explanation for the difference in this behavior is the difference in peak tracer concentrations introduced to dead zones, a function of the differential peak concentrations of the tracer plumes in each channel (Fig. 3).

For a particular dead zone, the tracer flux into it depends on its spatial context for two reasons. Firstly, initial loading of tracer differs downstream due to dispersion of the plume during transport, resulting in downstream dead zones being subject to a tracer plume that is lower in concentration and more broadly spread out in the thalweg than upstream dead zones. Secondly, partly related to variability in loading, after peak thalweg tracer concentrations have passed, flushed tracer from upstream dead zones will have the opportunity to exchange with downstream dead zones. This, too, is a heterogeneous process along the length of the reach because it depends in part on the exchange dynamics of each upstream dead zone. Dead zone BTC timing and magnitude is a function of the upstream solute transport process that provides the input boundary condition to a dead zone. Initial loading of tracer is a dominant process controlling dead zone BTCs because the concentration gradients between the thalweg and dead zones are greatest

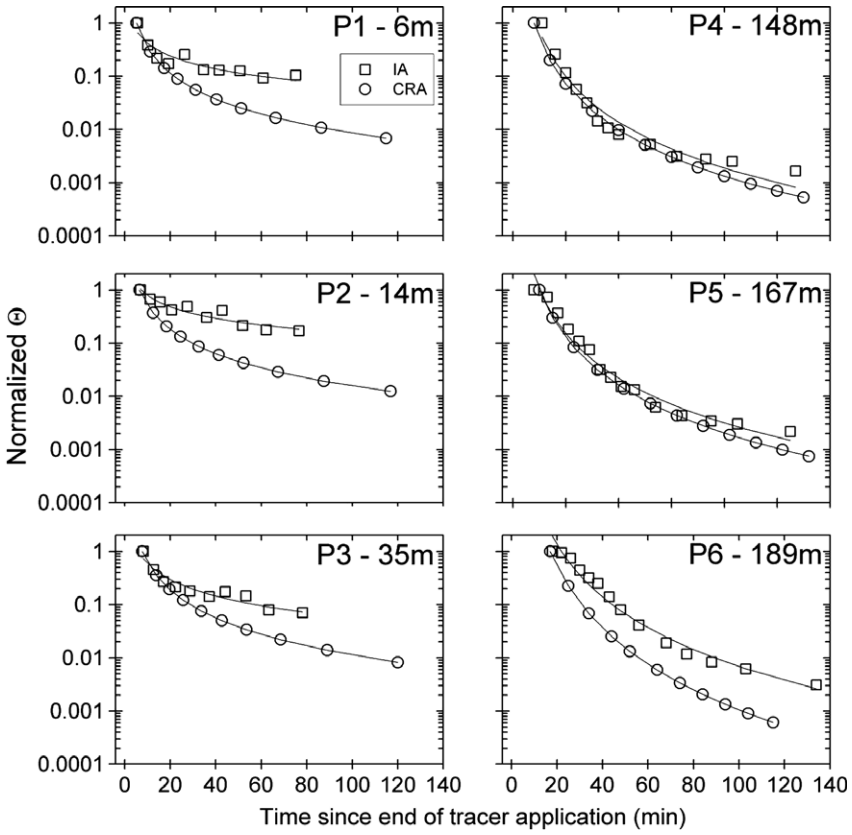

Figure 8 Normalized residence time functions Θ_{IA} and Θ_{CRA} from peat-lined reach dead zones (P1) eddy behind a boulder at 6 m, (P2) small side channel at 14 m, (P3) pool margin at 35 m, (P4) pool margin at 148 m, (P5) pool margin at 167 m, and (P6) pool margin at 189 m downstream of the injection location. Symbols represent discrete times of sampling, and lines are the functions identified in Table 1. All data are normalized to the first value being a Θ value of 1.0 for each time series.

as tracer in the thalweg is at its maximum, and dead zone concentrations are near background. IA and CRA experiments differ greatly in this respect. In the IA experiments conducted here, there was a substantial decrease in maximum stream tracer concentrations with distance downstream, from an estimated 900 $\mu g\,L^{-1}$ at head of experimental reach to $\sim$100 $\mu g\,L^{-1}$ at the downstream outlet (Fig. 3). Decreases in peak concentrations were expected as the tracer plume was dispersed with transport downstream, and consequently, potential primary loading of tracer also decreased with distance downstream. On the other hand, in the CRA experiments, the downstream decreases in maximum observed stream concentrations of tracer were more subtle, <13% (8.0 $\mu g\,L^{-1}$) in the alluvial reach and <12% (11.2 $\mu g\,L^{-1}$) in the peat reach (Fig. 3). Thus, in all experiments, peak concentrations from the downstream storage zones have lower concentrations than at upstream sites, forcing less curvature in the flushing responses of the downstream locations (Figs. 5 and 6). Because discharge conditions were similar during both the IA and CRA experiments on each reach, hydrodynamics at dead zone interfaces should not have been substantially different during these two experiment types. The general downstream increase of power-law exponents of regressions of dead zone BTCs for each experiment in both reaches indicates that downstream dead zone flushing is a function of upstream flushing and subsequent loading to these downstream dead zones. In both streams, the downstream dead zone BTC trends are more similar between IA and CRA results when compared to upstream observed dead zone BTCs.

The period after the main portion of the tracer plume has passed, represents a more complicated situation than during initial arrival of the tracer, as exchange is controlled by both tracer loading released from upstream storage zones and the local storage zone tracer flushing. Thus, in both experiment types, tracer concentration gradients between the thalweg and storage zones at downstream sites will decrease with time, but at slower rates than those of the upstream storage zones.

Further indication of the differential loading characteristics between IA and CRA experiments is observed in the comparison of the storage zone BTCs of both reaches. For the IA experiments, the exponent slopes of aggregate BTC regressions observed in dead zones all have greater magnitudes than those in the CRA experiments, indicating a steeper flushing slope or shorter aggregated residence time, which is to be expected given the preferential loading of high tracer concentrations to upstream storage zones during an IA experiment. These downstream shifts in dead zone loading and flushing are important, especially for the consideration of sampling dead zones for non-conservative stream tracers, because the effect or influence of reaction for any single dead zone is likely to be dependent upon the concentration of the non-conservative tracer. Thus, for the IA technique, dead zones are loaded with highly variable peak tracer concentrations, which may greatly confound

assessing the reactions occurring in upstream vs. downstream dead zones.

Ideally, assessment of dead zone RTDs to determine how dead zones function (i.e., as disaggregated signals from upstream influences) would be facilitated by measurements of dead zone volume, stream discharge near the dead zone, and detailed velocity distributions from the thalweg into the dead zone. Unfortunately, we did not collect this data at the time of the experiment and, given the remoteness of the sites, we were not able to re-visit the streams to collect such data. Future investigations of individual dead zone function would benefit from such measurements, as well as detailed measurements or characterizations of hydrodynamics (spatial velocity fields, etc.). Advancing our understanding of dead zone function would be particularly strong if such measurements were to be corroborated with RTD analysis as is demonstrated here.

Based on stream tracer BTCs observed in the thalweg and in hyporheic wells, Harvey et al. (1996) noted that the results of the CRA stream tracer technique are sensitive to the time scale of the injection and the spatial scale of sampling locations (i.e., influencing the ''window of detection'' of a tracer experiment). We did not sample the hyporheic zone, which would have likely resulted in the similar results to those of Harvey et al. (1996), because exchange time scales through porous media are likely to be slower than exchange through dead zones. However, the hyporheic zone is very heterogeneous, and samples from a few locations would not necessarily be representative of hyporheic dynamics overall. The advantage of sampling dead zones is that they are easily observed and are more likely to be well-mixed than the hyporheic zone. Additionally, a more representative collection of them can therefore be sampled, compared to a suite of hyporheic sampling locations (i.e., representative hyporheic locations are not easily observed). Thus, the dead zone storage sampling presented here allows for an analogous experimental design, complementary to the findings of Harvey et al. (1996).

It is interesting to note that the majority of the flushing responses of the dead zones are power-law responses. This is contrary to previous work by Uijttewaal et al. (2001), Hall et al. (2002), and Weitbrecht et al. (2008), all of whom suggested that dead zone storage should be exponential in behavior, assuming that storage zones are well-mixed. Because we did not sample all transient storage locations (i.e., all dead zones and all hyporheic locations) and because of the potential effects of downstream loading from upstream flushing (i.e., the influence of upstream tracer flushing time scales on downstream dead zone RTDs), we cannot definitively state that all dead zone storage flushing behaviors are power-law. Also, because we cannot disaggregate the individual dead zone from upstream behavior, we cannot ascertain if the power-law behavior is entirely driven by upstream processes. Again, we expect that the fundamental hydrodynamics driving exchange between dead zones and the main channel are similar in the IA and CRA experiments in both reaches. However, the reach scale response in the peat-bedded stream, as a cumulative response of all storage zones along the reach is different from the alluvial stream because it has an exponential rather than power-law RTD.

It has been established that RWT is not a perfectly conservative tracer (Bencala et al., 1983), particularly in groundwater studies (e.g., Sutton et al., 2001). However, the more popular method of using dissolved salt as a stream tracer does not allow for the same reliable low-concentration quantification of stream tracer, without increasing concentration to levels that would influence stream water density or cause ecologic disturbance. The added sensitivity of the RWT stream tracer method has also allowed for novel interpretation of long-term transient storage because RWT BTC tails have been observed in several mountain streams on the order of days after the tracer addition (Haggerty et al., 2002; Gooseff et al., 2003). We chose to use RWT because of the enhanced detection range of concentrations, which would allow for excellent characterization of BTC late time data in both IA and CRA experiments.

We expected there would not be substantial difference in stream response (RTDs) to IA and CRA stream tracer experiments, given the same discharge conditions. However, discharges were slightly different between IA and CRA experiments, which introduce some uncertainty in the comparison of the techniques. Discharges during IA and CRA experiments were within 3% and 10% of each other in the peat-bedded and alluvial reaches, respectively. These differences are within the expected error of the velocity-area stream gauging method, which allows for our assumption that the discharge conditions were similar between experiments. Similarity of RTDs between IA and CRA experiments from Payn et al. (2008) also strongly support relatively constant hydrologic conditions. However, the effect of discharge is important to stream transient storage (Zarnetske et al., 2007). If this change in discharge was influential, it is perhaps more pronounced in the alluvial reach than in the peat-bedded reach, because the difference in discharge during the two experiments was greater in the alluvial reach than in the peat-bed reach. Discharge changes in the steeper alluvial reach with a high width to depth ratio are likely to drive greater differences in the thalweg-dead zone connectivity than in the peat-bed reach, which has a low width to depth ratio (i.e., the water level is more likely to respond vertically than laterally to changes in discharge). Our results indicate that neither of the IA experiments influenced the results of the subsequent CRA experiments. This suggests that the few hours between each experiment (Fig. 2) were adequate to flush all of the detectable levels of the tracer mass from each reach.

Implications for future investigations

These results apply to general stream tracer experimental design. The similarity in whole-stream BTC regressions for IA and CRA results in two morphologically distinct reaches suggests that there is little difference between the two methods in assessing reach scale storage, further supporting the findings of Payn et al. (2008). The overall indication from this investigation is that generalizations about the different storage dynamics of streams require assessment of both whole-stream transport dynamics above the dead zone of interest and the processing of the dead zone itself. Parsing this information is necessary to separate the dead zone RTD from that of the upstream transport, and subsequently provide a more useful comparative assessment among

storage zones. Further, this work demonstrates that the variability of storage zone loading inherent in the IA method strongly influences storage zone exchange and interpretation of reach scale solute transport.

Our results also suggest that these two experiment techniques are sensitive to different characteristics of a stream that control transient storage, and the longitudinal distribution of transient storage zones. That is, a stronger, more attenuating storage zone in an upstream location is likely to modify the end-of-reach solute BTC differently than if it was located at the end of the reach, simply because of the effect such a feature would have on downstream tracer loading. Thus, IA and CRA measurement of internal reach processes are not similar enough to compare confidently among a group of reaches for which one or the other experiment was performed. Furthermore, there is an important potential bias that would result from variability in reach concentrations during an IA experiment in studies of non-conservative tracer behavior. For example, biogeochemically active tracer reactions or uptake processes, the subject of many stream tracer experiments, may be dependent upon proportional or non-linear functions of the tracer concentration. Consistency in achieving downstream target thalweg concentrations in IA experiments is difficult because empirical mixing equations (e.g. Fisher et al., 1979) are not always appropriate for a given reach. Furthermore, repeated IA experiments at different discharges, even in the same reach, are likely to result in different BTC responses (e.g., Zarnetske et al., 2007) simply because the longitudinal distribution of peak thalweg concentrations will not be similar for each experiment. Therefore, neither will the pattern of loading to storage zones downstream, an effect that cannot be easily distinguished from actual changes in transient storage dynamics. On the other hand, in CRA experiments, there is generally a smaller disparity in thalweg tracer concentrations longitudinally, and if discharge can be estimated, it is generally easier to predict peak downstream tracer concentrations. Thus, CRA experiments result in a more consistent loading of all storage zones along a reach, and comparable loading of tracer. Therefore, CRA experiments may provide a more representative and inter-site comparable characterization of the internal mechanisms of stream solute transport. This is consistent with Wagner and Harvey (1997), who noted that CRA experiments are better for identifying particular mechanisms of transient storage. CRA experiments also provide more uniform and constant reach concentrations that would simplify kinetic modeling of active tracer behavior.

Conclusions

Previous studies of stream tracer experiment design (Harvey et al., 1996) and transient storage model performance (Wagner and Harvey, 1997) suggest that there are physical limitations to stream tracer experiment design. The performance of solute transport models at various time scales of experiments suggests that parameters of transient storage models are insensitive to measured process if the travel time of the experiment is incompatible with rates of mobile–immobile exchange. To better understand the rates of internal mass transfers driving these observations, we incorporated sensitive tracer techniques to compare of IA and CRA tracer experiments in two streams of different channel structure and bed material. We show that there are differences in the loading and flushing BTC dynamics of IA and CRA techniques among in-channel dead zones, as well as in the dead zone aggregate RTDs. The main reason for the difference between dead zone IA and CRA experiments is the difference in loading behavior in each experiment type. This finding has important implications for design of stream tracer experiments because it suggests that there will be substantial differences between IA and CRA experiments that include non-conservative tracers, and, more importantly, the conclusions drawn from simulations of each.

Acknowledgements

The authors would like to thank Ken Hill for laboratory assistance, the Toolik Lake Research Station staff, VECO Polar, and Air Logistics for logistical field support and two anonymous reviewers whose comments greatly improved this manuscript. This work was supported by NSF grant no. OPP 03-27440.

References

Bencala, K.E., Rathbun, R.E., Jackman, A.P., Kennedy, V.C., Zellweger, G.W., Avanzino, R.J., 1983. Rhodamine WT dye losses in a mountain stream environment. Water Resources Bulletin 19 (6), 943–950.

Bradford, J.H., McNamara, J.P., Bowden, W.B., Gooseff, M.N., 2005. Imaging depth-of-thaw beneath arctic streams using ground-penetrating radar. Hydrological Processes 19, 2689–2699.

Brosten, T., Bradford, J.H., McNamara, J.P., Zarnetske, J.P., Gooseff, M.N., Bowden, W.B., 2006. Profiles of temporal thaw depths beneath two arctic stream types using ground-penetrating radar. Permafrost and Periglacial Processes 17 (4), 341–355.

Ensign, S.H., Doyle, M.W., 2005. In-channel transient storage and associated nutrient retention: evidence from experimental manipulations. Limnology and Oceanography 50 (6), 1740–1751.

Fisher, H.B., List, J.E., Koh, C.R., Imberger, J., Brooks, N.H., 1979. Mixing in Inland and Coastal Waters. Elsevier, The Netherlands, p. 302.

Gooseff, M.N., Wondzell, S.M., Haggerty, R., Anderson, J., 2003. Comparing transient storage modeling and residence time distribution (RTD) analysis in geomorphically varied reaches in the Lookout Creek basin, OR, USA. Advances in Water Resources 26 (9), 925–937.

Gooseff, M.N., LaNier, J., Haggerty, R., Kokkeler, K., 2005. Determining in-channel (dead zone) transient storage by comparing solute transport in a bedrock channel–alluvial channel sequence, Oregon. Water Resources Research 41, W06014. doi:10.1029/2004WR003513.

Haggerty, R., Wondzell, S.M., Johnson, M.A., 2002. Power-law residence time distribution in the hyporheic zone of a 2nd-order mountain stream. Geophysical Research Letters 29. doi:10.1029/2002GL014743.

Haggerty, R., Reeves, P.C., 2002. STAMMT-L Version 1.0 User's Manual. Sandia National Laboratories. Albuquerque, New Mexico, 76pp.

Hall, R.O., Bernhardt, E.S., Likens, G.E., 2002. Relating nutrient uptake with transient storage in forested mountain streams. Limnology and Oceanography 47, 255–265.

Harvey, J.W., Wagner, B.J., Bencala, K.E., 1996. Evaluating the reliability of the stream tracer approach to characterize stream-subsurface water exchange. Water Resources Research 32, 2441—2451.

Payn, R.A., Gooseff, M.N., Benson, D.A., Cirpka, O.A., Zarnetske, J.P., Bowden, W.B., McNamara, J.P., Bradford, J.H., 2008. Comparison of instantaneous and constant-rate stream tracer experiments through non-parametric analysis of residence time distributions. Water Resources Research 44, W06404, doi:10.1029/2007WR006274.

Sutton, D.J., Kabala, Z.J., Francisco, A., Vasudevan, D., 2001. Limitations and potential of commercially available rhodamine WT as a groundwater tracer. Water Resources Research 37, 1641—1656.

Uijttewaal, W.S.J., Lehmann, D., van Mazijk, A., 2001. Exchange processes between a river and its groyne fields: model experiments. Journal of Hydraulic Engineering 127 (11), 928—936.

Wagner, B.J., Harvey, J.W., 1997. Experimental design for estimating parameters of rate-limited mass transfer: analysis of stream tracer studies. Water Resources Research 33, 1731—1741.

Weitbrecht, V., Socolofsky, S.A., Jirka, G.H., 2008. Experiments on mass exchange between groin fields and main stream in rivers. Journal of Hydraulic Engineering 134, 173—183.

Wondzell, S.M., 2006. Effect of morphology and discharge on hyporheic exchange flows in two small streams in the Cascade Mountains of Oregon, USA. Hydrological Processes 20, 267—287.

Zarnetske, J.P., Gooseff, M.N., Brosten, T.R., Bradford, J.H., McNamara, J.P., Bowden, W.B., 2007. Transient storage as a function of geomorphology, discharge, and permafrost active layer conditions in arctic tundra streams. Water Resources Research 43, W07410. doi:10.1029/2005WR004816.

Zarnetske, J.P., Gooseff, M.N., Bowden, W.B., Greenwald, M.J., Brosten, T.R., Bradford, J.H., McNamara, J.P., 2008. Influence of morphology and permafrost dynamics on hyporheic exchange in Arctic headwater streams under warming climate conditions. Geophysical Research Letters 35, L02501. doi:10.1029/2007GL032049.